EUROPEAN JOURNAL OF PURE AND APPLIED MATHEMATICS
2025, Vol. 18, Issue 3, Article Number 6670
ISSN 1307-5543 – ejpam.com
Published by New York Business Global

Numerical Assessment of the Hepatitis B Virus Transmission Model Using a Non-standard Finite Difference Scheme and a Feedforward Neural Network

Tahir Khan[1], II Hyo Jung[1,*], Gul Zaman[2], Ilyas Khan[3]

[1] *Department of Mathematics/Institute of Mathematical Science, Pusan National University, Busan, Republic of Korea*
[2] *Department of Mathematics, University of Malakand Chakdara, Dir (L), Pakhtunkhwa, Pakistan*
[3] *Faculty of Mathematics and Statistics, Ton Duc Thang University, Ho Chi Minh City, Vietnam*

Abstract. Hepatitis B virus (HBV) infection is one of the leading causes of death and is a contagious disease that produces chronic liver infection. The infection of hepatitis B has a complex nature involving multiple and long infectious periods, behavioral changes, and healthcare limitations. The multiple infection phases, immune system, behavioral changes, and healthcare saturation have a significant impact on the dynamics of hepatitis B virus transmission. Since HBV can persist in the body for years, the number of infectious individuals accumulates, and people take precautionary measures as awareness increases. Considering the multiple stages of the disease and the saturation level, we propose an innovative hybrid approach combining a mathematical model with a saturated incidence rate and a forward neural network to represent the transmission dynamics of the hepatitis B virus. First, we prove the biological and mathematical feasibility to show that the model under consideration is well-posed. We also investigate the dynamics of the model using linear stability analysis to derive the stability conditions. In addition, we perform the numerical assessment of the model using a novel hybrid approach of NSFD–FFNN framework to show the accuracy and large-scale numerical simulations.

2020 Mathematics Subject Classifications: 92D30, 65L12, 65M06, 68T07

Key Words and Phrases: Stability analysis, non-standard finite difference scheme, feed-forward neural network, numerical simulations

1. Introduction

Living things, particularly humans, are constantly at risk from infectious diseases. Every person may experience an infectious disease once or multiple times during their

*Corresponding author.
DOI: https://doi.org/10.29020/nybg.ejpam.v18i3.6670

Email addresses: tahirmaths200014@gmail.com (T. Khan), ilhjung@pusan.ac.kr (I. H. Jung), gzaman@uom.edu.pk (G. Zaman), ilyaskhanqau@yahoo.com (I. Khan)

lifetime. The infection could be acute or chronic, i.e., short-term or long-term, but cause mortality. The second leading cause of death and disability in human beings and other living organisms is infectious diseases around the globe, according to the WHO. In the current century, millions of people suffer due to the consequences of infectious diseases. Among these are tuberculosis, diarrheal diseases, malaria, hepatitis, HIV/AIDS, etc. The liver is one of the important organs in the human body, located in the upper right-hand part of the abdomen. Hepatitis B is one of the severe types of hepatitis that produces inflammation of the liver and leads to cirrhosis [1]. Hepatitis B is transmitted from one individual to another by direct contact or indirect contact [2]. Hepatitis B virus (HBV) infection progresses through multiple phases, most notably the acute and chronic stages, which are critical in understanding its clinical and epidemiological impact. During the acute phase, individuals often remain asymptomatic and may recover spontaneously without the need for antiviral treatment. However, a subset of infected individuals fail to clear the virus, leading to the development of a chronic infection, which may persist for life [3]. Globally, an estimated 300 million people are chronic carriers of HBV, facing significantly increased risks of HBV-related mortality. Known as a silent killer, HBV frequently progresses unnoticed, particularly in its chronic form. The acute phase typically lasts up to six months, during which the immune system may successfully eliminate the virus from the host. In contrast, the chronic phase is more severe and symptomatic, with the virus persisting in the body. This long-term infection can lead to serious complications, including liver cirrhosis and liver failure [4, 5]. While antiviral treatment is generally unnecessary during the acute phase, where rest, hydration, and proper nutrition are recommended—immediate medical intervention becomes essential if the infection progresses to the chronic stage.

Mathematical modeling refers to the process of representing real-world phenomena using mathematical expressions, and it is widely applied across various disciplines, including physics, computer science, and biology [6–9]. In the context of epidemiology, mathematical models play a crucial role in understanding the transmission dynamics of infectious diseases, evaluating control strategies, and predicting both short and long-term outcomes [10, 11]. These models consist of differential equations, which describe a framework to show the temporal evolution of disease spread (see, e.g., [12, 13]). However, analyzing the mathematical properties of such models and finding their exact or approximate solutions is challenging, but one must also look for alternative approaches while dealing with their solutions. To address this, alternative computational techniques, particularly neural network-based methods, have been increasingly employed to obtain accurate and efficient solutions. Given that many real-world systems are inherently governed by differential equations, solving them using neural networks is an emerging and rapidly growing field of research [14]. In recent years, significant progress has been made, highlighting the promising interplay between neural networks and differential equation solvers [15].

Neural networks are computational models inspired by the architecture and functioning of the human brain. They consist of interconnected artificial neurons organized into multiple layers, typically including an input layer, one or more hidden layers, and an output layer [16]. Input data passes through these layers, where mathematical operations

produce an output. Each artificial neuron processes incoming signals by applying weighted sums to the inputs, followed by the application of an activation (or merit) function, which introduces nonlinearity and determines whether the signal passes to the next layer. This layered structure enables the network to learn and model complex, nonlinear relationships in data. Among neural network architectures, the feed-forward neural network (FFNN) is particularly significant. In FFNNs, data flows in one direction from input to output, without feedback loops. They are widely used in the analysis of epidemiological models, where they approximate nonlinear dynamics involved in the transmission of infectious diseases. By learning from data, FFNNs offer a powerful, data-driven approach for forecasting disease trends and enhancing the understanding of epidemic processes with high predictive accuracy. With the aid of nonlinear activation functions and multiple layers of neurons, FFNNs can approximate the disease transmission mechanisms to help estimate the key epidemic parameters (infection rate, recovery rate, and transmission probability). Moreover, FFNNs are highly adaptable and can integrate real-world datasets, including time series infection data, demographic information, and vaccination, making them more effective in forecasting outbreaks in uncertain environments. When applied to epidemiological models, FFNNs improve predictive accuracy, decision-making, intervention strategies, policy implementation, assisting public health authorities in resource allocation, and early warning for outbreaks. Various neural network procedures are utilized to analyze the models as reported in [17–19]. However, the proposed epidemiological problem has never been considered or solved with the help of the proposed approaches.

The main objective of the proposed work is to introduce a model representing the dynamics of the hepatitis B virus with reasonable assumptions and to analyze it with the aid of dynamical system theory, non-standard finite difference (NSFD) scheme, and feed-forward neural network (FFNN) framework. Precisely, we have the following contributions.

1. Since the multiple phases of hepatitis B have a significant impact on the transmission dynamics of the disease, we will consider the different infectious phases (latent, acute, and chronic) of the disease while formulating the proposed model.

2. Incorporating the saturated incidence rate is also an important consideration of the proposed work because the bilinear incidence only assumes that the incidence rate is proportional to the amount of susceptible and infectious population; however, this is not the case in hepatitis B virus transmission. Besides this one, the saturated incidence assumes the fact that transmission may plateau as the ratio of the infectious population reaches a certain threshold. Because the virus persists in individuals for a long time, the ratio of infected individuals may not be directly proportional to the number of susceptible individuals.

3. The framework of NSFD and FFNN will be utilized to present the accurate dynamics and to show the close match between predicted and true values, as well as to investigate the robustness of the proposed framework while modeling the dynamics of HBV.

The paper is organized as follows. The detailed formulation of the model is provided

in section 2. We also discuss the biological and mathematical feasibility of the model in subsection 2.1. We linearize the proposed model and find the reproductive number in subsections 2.2 and 2.3 respectively. The dynamical properties of the model take place in subsections 2.4 and 2.5. We provide the framework of the NSFD and FFNN in section 3. We conclude our work in section 4.

2. Mathematical model formulation

In this section, we will present an epidemic model for the transmission of HBV. Keeping the complex nature and multiple phases of HBV according to the disease characteristics, we assume three infected population groups of latently, acutely and chronically infected populations to acknowledge the biological importance of the latent, acute and chronic stage in HBV infection. Moreover, the infection has long infectious periods and can persist in the body for years, and as awareness increases, the people take precautionary measures, so the number of infectious individuals accumulates, therefore, we use saturated incidence rate $\beta SI/(1+\gamma I)$, to better reflects the transmission scenarios. The susceptible individuals may transition to latent, acute and then chronically infected group of population after successful interaction with the infected individual. Since, there is no need of proper treatment in acute stage and those who recover naturally will transit to recover compartment, however, those who produce complication will leads to chronically infected population group. These infected individuals leave their compartments due death or full recovery. Parentally infected individuals will directly transit to chronically infected population. Vaccine of hepatitis B are also very effective and provide immunity, so those who vaccinated successfully will transit to vaccinated compartment. Thus, the total population groups are distributed in six epidemiological subclasses i.e. s, l, a, c, r and v respectively, represent the susceptible, latent, acute infected, chronic carrier infectious, recovered and vaccinated individuals, whose the schematic process of the disease propagation among different epidemiological groups of population is illustrated by a flowchart as given in Figure 1. Eventually, the dynamics of these compartments are governed by the following system of nonlinear differential equations:

$$\begin{cases} \dfrac{ds(t)}{dt} = g\eta(1-\varphi c(t)) + \pi v(t) - \dfrac{\alpha s(t)a(t)}{1+\beta c(t)} - \dfrac{\lambda\alpha s(t)c(t)}{1+\beta c(t)} - (\mu_0+\lambda_3)s(t), \\ \dfrac{dl(t)}{dt} = \dfrac{\alpha s(t)a(t)}{1+\beta c(t)} + \dfrac{\lambda\alpha s(t)c(t)}{1+\beta c(t)} - (\mu_0+\theta)l(t), \\ \dfrac{da(t)}{dt} = \theta l(t) - (\mu_0+\lambda_1)a(t), \\ \dfrac{dc(t)}{dt} = g\eta\varphi c(t) + q\lambda_1 a(t) - (\mu_0+\mu_1+\lambda_2)c(t), \\ \dfrac{dr(t)}{dt} = \lambda_2 c(t) + (1-q)\lambda_1 a(t) - \mu_0 r(t), \\ \dfrac{dv(t)}{dt} = g(1-\eta) + \lambda_3 s(t) - (\mu_0+\pi)v(t), \end{cases} \tag{1}$$

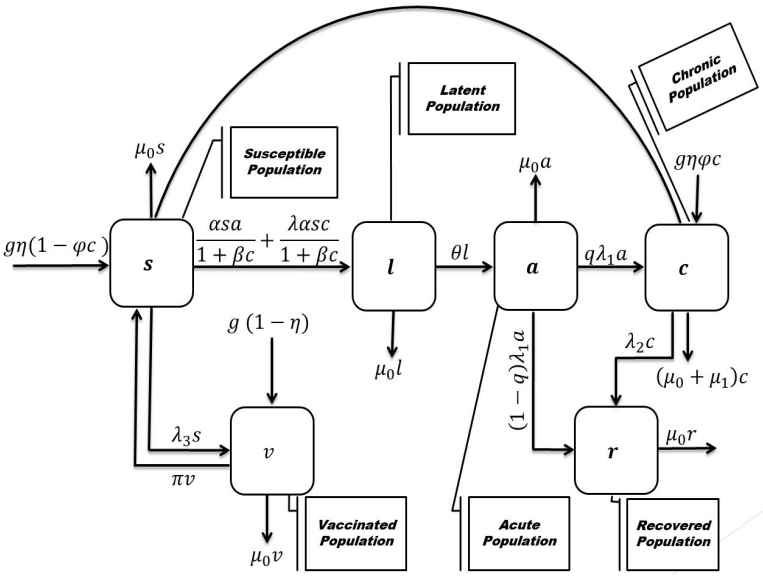

Figure 1: The plot represent the schematic process of the HBV propagation among different epidemiological groups of population.

along with non-negative initial population sizes

$$s(0), \quad v(0) > 0, \quad l(0), \quad a(0), \quad c(0), \quad r(0) \geq 0. \tag{2}$$

In the model (1), g represents the birth rate while the rate of birth without successful vaccination is represented by η. The quantity of maternally distorted individuals is denoted by φ, and the rate of waning vaccine-induced immunity is π. We symbolize the transmission rate from susceptible to infected, denoted by the parameters α and λ, as the reduced transmission rate. μ_0 represents rate of natural death. The rate of vaccination is λ_3, and the amount at which the latent individuals lead to acute class is represented by θ. In contrast, the portion of individuals who transition from the acute population to the chronic carrier is represented by λ_1. We also denote the rate at which the individuals move from chronic carrier to the immune class by λ_2, and the parameter μ_1 is the death that occurs from hepatitis B. Moreover, we assume that q is the average rate of those individuals who become unsuccessful in recovering from hepatitis B in the primary stage of hepatitis B (acute) and move to the chronic stage.

Having presented the detailed model formulation, we proceed to analyze the proposed epidemic model by establishing its well-posedness, ensuring that it is both biologically and mathematically meaningful.

2.1. Well-posedness

We discuss the well-posedness of the proposed system to show that the epidemic model is feasible in both senses, biologically and mathematically. For this, we assume that the total population is represented by $n(t)$ with $n = v+l+a+s+r+c$. The model (1), together

with initial conditions (2) satisfies that $n(t) \geq 0$ implies that $n(t)$ (total population) is bounded and positive for $t > 0$, thus the time derivative of $n(t)$ gives

$$\frac{dn(t)}{dt} = g - \mu_0 n(t) - \mu_1 c(t), \tag{3}$$

which shows that as $t \to \infty$, $n(t) \leq \frac{g}{\mu_0}$, hence

$$\Omega = \left\{ (s(t), l(t), a(t), c(t), r(t), v(t)) \in \mathcal{R}_+^6, n(t) \leq \frac{g}{\mu_0} \right\}. \tag{4}$$

is the feasible region.

To show the existence analysis, we can express the proposed epidemic problem as initial value problem as follows:

$$\mathcal{H}^{'}(t) = \mathcal{F}(y), \quad y(0) = y_0, \tag{5}$$

where $y = (s, l, a, c, r, v)^t$ and $\mathcal{F} = (f_1, f_2, \ldots, f_6)^t$. To proceed further, we recall the definition of Lipschitz continuity as follows.

Definition 1. *[20] The function $\mathcal{F}(y)$ is said to be Lipschitz continuous if there exists a constant $\mathcal{M} > 0$ such that*

$$\|\mathcal{F}(y_1) - \mathcal{F}(y_2)\| \leq \mathcal{M}\|y_1 - y_2\|.$$

Thus, regarding existence of solution, we prove the following proposition.

Proposition 2.1. There exists a unique solution of the system (5) analogous to the proposed model (1) and (2).

Proof. To show that the model posses a unique solution, it is sufficient to prove that the function $\mathcal{F}(y)$ satisfies the Lipschitz condition provided in the above definition. Keeping in mind the set Ω and $n(t) \leq g/\mu_0$, which implies that all the state variables for $i = 1, 2$, s_i, l_i, a_i, c_i, r_i and v_i are bounded. One can proceed as follows:

$$\begin{aligned}\|f_1(y_1) - f_1(y_2)\| = \Bigg\| & g\eta\varphi(c_2 - c_1) + \pi(v_1 - v_2) - \alpha\left(\frac{s_1 a_1}{1+\beta c_1} - \frac{s_2 a_2}{1+\beta c_2}\right) \\ & -\lambda\alpha\left(\frac{s_1 c_1}{1+\beta c_1} - \frac{s_2 c_2}{1+\beta c_2}\right) - (\mu_0 + \lambda_3)(s_1 - s_2)\Bigg\|,\end{aligned}$$

which implies that

$$\begin{aligned}\|f_1(y_1) - f_1(y_2)\| \leq & g\eta\varphi\|c_1 - c_2\| + \pi\|v_1 - v_2\| + (\mu_0 + \lambda_3)\|s_1 - s_2\| \\ & + \alpha\left\|\frac{s_1 a_1}{1+\beta c_1} - \frac{s_2 a_2}{1+\beta c_2}\right\| + \lambda\alpha\left\|\frac{s_1 c_1}{1+\beta c_1} - \frac{s_2 c_2}{1+\beta c_2}\right\|. \end{aligned} \tag{6}$$

To simplify the above inequality, we use some algebraic manipulation as follows

$$\begin{aligned}\frac{s_1 a_1}{1+\beta c_1} - \frac{s_2 a_2}{1+\beta c_2} &= \frac{s_1 a_1 - s_2 a_2}{1+\beta c_1} - s_2 a_2\left(\frac{1}{1+\beta c_1} - \frac{1}{1+\beta c_2}\right), \\ \frac{s_1 c_1}{1+\beta c_1} - \frac{s_2 c_2}{1+\beta c_2} &= \frac{s_1 c_1 - s_2 c_2}{1+\beta c_1} - s_2 c_2\left(\frac{1}{1+\beta c_1} - \frac{1}{1+\beta c_2}\right).\end{aligned}$$

Also

$$\|s_1a_1 - s_2a_2\| \leq \|s_1\|\|a_1 - a_2\| + \|a_2\|\|s_1 - s_2\|,$$
$$\|s_1c_1 - s_2c_2\| \leq \|s_1\|\|c_1 - c_2\| + \|c_2\|\|s_1 - s_2\|,$$

and

$$\left\|\frac{1}{1+\beta c_1} - \frac{1}{1+\beta c_2}\right\| \leq \frac{\beta\|c_1 - c_2\|}{\|(1+\beta c_1)(1+\beta c_2)\|} \leq \beta\|c_1 - c_2\|.$$

Using the above algebraic manipulations, the equation (6) leads to the following inequality

$$\begin{aligned}\|f_1(y_1) - f_1(y_2)\| \leq \big\{\mu_0 + \lambda_3 + \alpha\|a_2\| + \lambda\alpha\|c_2\|\big\}\|s_1 - s_2\| + \alpha\|s_1\|\|a_1 - a_2\| \\ + \big\{g\eta\varphi + \alpha\beta\|s_2\|\|a_2\| + \alpha\beta\lambda\|s_2\|\|c_2\| + \alpha\lambda\|s_1\|\big\}\|c_1 - c_2\| + \pi\|v_1 - v_2\|.\end{aligned}$$

Let us assume that the $\mathcal{M}_1$, $\mathcal{M}_2$ and $\mathcal{M}_3$ are any positive constants, then the above equation takes the form

$$\|f_1(y_1) - f_1(y_2)\| \leq \mathcal{M}_1\|s_1 - s_2\| + \mathcal{M}_2\|a_1 - a_2\| + \mathcal{M}_3\|c_1 - c_2\| + \pi\|v_1 - v_2\|.$$

Let $\mathcal{M} = \max\{\mathcal{M}_1, \mathcal{M}_2, \mathcal{M}_3, \pi\}$, the last inequality can be re-written as

$$\|f_1(y_1) - f_1(y_2)\| \leq \mathcal{M}\big(\|s_1 - s_2\| + \|a_1 - a_2\| + \|c_1 - c_2\| + \|v_1 - v_2\|\big) \leq \mathcal{M}\|y_1 - y_2\|. \quad (7)$$

The second equation of the model (1), implies that

$$\begin{aligned}\|f_2(y_1) - f_2(y_2)\| \leq \big\{\alpha\|a_2\| + \lambda\alpha\|c_2\|\big\}\|s_1 - s_2\| + (\mu_0 + \theta)\|l_1 - l_2\| + \alpha\|s_1\|\|a_1 - a_2\| \\ + \big\{\alpha\beta\|s_2\|\|a_2\| + \alpha\beta\lambda\|s_2\|\|c_2\| + \alpha\lambda\|s_1\|\big\}\|c_1 - c_2\|.\end{aligned}$$

If $\mathcal{N}_1$, $\mathcal{N}_2$, $\mathcal{N}_3$ and $\mathcal{N}_4$ are positive constants, and $\mathcal{N} = \max\{\mathcal{N}_1, \mathcal{N}_2, \mathcal{N}_3, \mathcal{N}_4\}$, then the above inequality gives

$$\|f_2(y_1) - f_2(y_2)\| = \mathcal{N}\big\{\|s_1 - s_2\| + \|l_1 - l_2\| + \|\|a_1 - a_2\| + \|c_1 - c_2\| \leq \mathcal{N}\|y_1 - y_2\|\big\}. \quad (8)$$

From the third equation of the model (1), we obtain

$$\|f_3(y_1) - f_3(y_2)\| \leq \theta\|l_1 - l_2\| + (\mu_0 + \lambda_1)\|a_1 - a_2\| \leq \mathcal{O}\|y_1 - y_2\|, \quad (9)$$

where $\mathcal{O} = \{\theta, (\mu_0 + \lambda_1)\}$. The fourth equation of the model (1) implies that

$$\|f_4(y_1) - f_4(y_2)\| \leq q\lambda_1\|a_1 - a_2\| + (g\eta\varphi + \mu_0 + \mu_1 + \lambda_2)\|c_1 - c_2\| \leq \mathcal{P}\|y_1 - y_2\|, \quad (10)$$

where $\mathcal{P} = \{q\lambda_1, (g\eta\varphi + \mu_0 + \mu_1 + \lambda_2)\}$. In a similar way, the last two equation of the proposed model gives

$$\begin{aligned}\|f_5(y_1) - f_5(y_2)\| \leq (1-q)\lambda_1\|a_1 - a_2\| + \lambda_2\|c_1 - c_2\| + \mu_0\|r_1 - r_2\| \leq \mathcal{Q}\|y_1 - y_2\|, \\ \|f_6(y_1) - f_6(y_2)\| \leq \lambda_3\|s_1 - s_2\| + (\mu_0 + \pi)\|v_1 - v_2\| \leq \mathcal{S}\|y_1 - y_2\|,\end{aligned} \quad (11)$$

where $\mathcal{Q} = \{(1-q)\lambda_1, \lambda_2, \mu_0\}$ and $\mathcal{S} = \{\lambda_3, (\mu_0 + \pi)\}$. Combining equation (7) to (11), we obtain

$$\|\mathcal{F}(y_1) - \mathcal{F}(y_2)\| = \mathcal{H}\|y_1 - y_2\|,$$

where $\mathcal{H} = \max\{\mathcal{M}, \mathcal{N}, \mathcal{O}, \mathcal{P}, \mathcal{Q}, \mathcal{S}\}$, ensure that the function $\mathcal{F}(y)$ is Lipschitz continuous, and hence the model posses a unique solution.

Proposition 2.2. Let us consider that $(s(t), l(t), a(t), c(t), r(t), v(t))$ is the solution of the model with non-negative initial conditions, and the closed set Ω is the attracting under the flow described by equation (1) that is positive invariant.

Proof. Let us assume a function $\mathcal{L}(t)$ given by

$$\mathcal{L}(t) = s(t) + l(t) + a(t) + c(t) + r(t) + v(t), \tag{12}$$

then the time differentiation with the implementation of equation (1) leads to

$$\frac{d\mathcal{L}(t)}{dt} = g - \mu_0 l(t) - \mu_1 c(t), \tag{13}$$

which implies that

$$\frac{d\mathcal{L}(t)}{dt} \leq g - \mu_0 l(t) \leq 0. \tag{14}$$

It is clear from the equation (14), that $\frac{d\mathcal{L}(t)}{dt} \leq 0$, which indicates that the set φ is positively invariant. Also, $0 \leq l(t) \leq l(0)e^{-\mu_0 t} + \frac{g}{\mu_0}(1 - e^{-\mu_0 t})$. Thus, as $t \to \infty$, $0 \leq \mathcal{L}(t) \leq \frac{g}{\mu_0}$, which is sufficient to prove that Ω is an attracting set.

The above proposition confirms that the proposed model is well-posed. We now proceed with the linearization of the model, computation of the threshold quantity, identification of the model equilibria, and its stability analysis, as outlined below.

2.2. Linearization of the model

Using the methods of dynamical systems to linearize the model that is under consideration. To make our calculation simpler, we take the Jacobian matrix of the reduced system (without the 5th equation), which looks like

$$J = \begin{bmatrix} -x_{11} & 0 & -x_{13} & x_{14} & \pi \\ x_{21} & -x_{22} & x_{23} & -x_{24} & 0 \\ 0 & \theta & -x_{33} & 0 & 0 \\ 0 & 0 & q\lambda_1 & -x_{44} & 0 \\ \lambda_3 & 0 & 0 & 0 & -x_{55} \end{bmatrix},$$

where

$$x_{11} = \frac{\alpha a(t)}{1+\beta c(t)} + \frac{\lambda\alpha c(t)}{1+\beta c(t)} + \mu_0 + \lambda_3, \quad x_{13} = \frac{\alpha s(t)}{1+\beta c(t)} = x_{23},$$
$$x_{14} = \frac{\beta\alpha s(t)a(t)}{1+\beta c(t)^2} - \frac{\lambda\alpha s(t)}{1+\beta c(t)^2} = -x_{24}, \quad x_{21} = x_{11} - (\mu_0 + \lambda_3),$$
$$x_{22} = \mu_0 + \theta, \quad x_{33} = \mu_0 + \lambda_1, \quad x_{44} = g\eta\varphi - \mu_0 - \mu_1 - \lambda_2, \quad x_{55} = \mu_0 + \pi.$$

2.3. Basic reproduction number

In epidemiological models, the threshold quantity, called the disease's basic reproduction number, is an essential quantity which describes the predicted average rate of infections induced by a single infective after introducing into an entirely susceptible community. To calculate this quantity for the proposed problem, we follow the methodology introduced by Watmough and Driessche [21], therefore assume that $y = (l(t), a(t), c(t))$, then the model (1) yields

$$\frac{dy}{dt} = F - V. \tag{15}$$

In equation (15), the matrices are define as:

$$F = \begin{bmatrix} \frac{\beta s(t)a(t)}{1+\beta c(t)} + \frac{\lambda\alpha s(t)c(t)}{1+\beta c(t)} \\ 0 \\ 0 \end{bmatrix},$$

$$V = \begin{bmatrix} (\theta+\mu_0)l(t) \\ (\mu_0+\lambda_1)a(t) - \theta l(t) \\ (\mu_0+\mu_1+\lambda_2)c(t) - q\lambda_1 a(t) - g\eta\varphi c(t) \end{bmatrix}.$$

Let $\mathcal{F}$ and $\mathcal{V}$ are the Jacobian of F and V at $\mathcal{F}_0$, then it becomes

$$\mathcal{F} = \text{Jacobian of } F = \begin{bmatrix} 0 & \alpha s_0 & \lambda\alpha s_0 \\ 0 & 0 & 0 \\ 0 & 0 & 0 \end{bmatrix},$$

$$\mathcal{V} = \text{Jacobian of } V = \begin{bmatrix} x_{11} & 0 & 0 \\ -\theta & x_{22} & 0 \\ 0 & -q\lambda_1 & x_{33} \end{bmatrix},$$

where $x_{11} = \theta + \mu_0$, $x_{22} = \mu_0 + \lambda_1$ and $x_{33} = \mu_0 + \mu_1 + \lambda_2 - g\eta\varphi$. ˜Thus, the basic reproductive number r_0 is the spectral radius of $K = \mathcal{F}\mathcal{V}^{-1}$ ($r_0 = \rho(\mathcal{F}\mathcal{V}^{-1})$). So the basic reproductive quantity r_0 of our suggested model (1) looks like

$$r_0 = r_1 + r_2, \tag{16}$$

where

$$r_1 = \frac{\theta\alpha s_0}{(\mu_0+\theta)(\mu_0+\lambda_1)},$$
$$r_2 = \frac{\theta\alpha s_0\lambda\lambda_1 q}{(\mu_0+\theta)(\mu_0+\lambda_1)(\mu_0+\mu_1+\lambda_2-g\eta\varphi)}.$$

2.4. Equilibrium analysis

To study the dynamics of the model that is under consideration (1), we first find the model equilibria. For this, we assume that the infection-free state of system (1) is

symbolized by $\mathcal{F}_0$ and $\mathcal{F}_0 = (s_0, 0, 0, 0, 0, v_0)$, where

$$s_0 = \frac{g\{\pi + \eta\mu_0\}}{\mu_0\{\pi + \mu_0 + \lambda_3\}}, \quad v_0 = \frac{g\{\mu_0 - \mu_0\eta + \lambda_3\}}{\mu_0\{\pi + \lambda_3 + \mu_0\}}. \tag{17}$$

Similarly, to find the endemic states of the model, we assume $\mathcal{P}_1 = (\mu_0+\lambda_3)$, $\mathcal{P}_2 = (\mu_0+\theta)$, $\mathcal{P}_3 = (\mu_0 + \lambda_1)$, $\mathcal{P}_4 = (\mu_0 + \mu_1 + \lambda_2 - g\eta\varphi)$ and $\mathcal{P}_5 = (\mu_0 + \pi)$ for the shake of simplicity, then the endemic state becomes $F_1 = (s^*, l^*, a^*, c^*, r^*, v^*)$, where

$$\begin{aligned}
s^* &= \frac{\{\mathcal{P}_5 g\eta + \pi g(1-\eta)\}}{\{\mathcal{P}_1 P_5 - \pi\lambda_3\}}, \quad l^* = \frac{\mathcal{P}_2\mathcal{P}_3\mathcal{P}_4\mu_0\{\mu_0 + \pi + \lambda_3\}(r_0 - 1) + \mathcal{P}_2\mathcal{P}_3\mathcal{P}_4\pi\lambda_3}{\mathcal{P}_2\theta\{\mathcal{P}_4\mathcal{P}_5\alpha + \mathcal{P}_5\lambda\alpha q\lambda_1 + \mathcal{P}_1\mathcal{P}_5\beta q\lambda_1 - \beta q\lambda_1\pi\lambda_3\}}, \\
a^* &= \frac{\mathcal{P}_2\mathcal{P}_4\mu_0\{\mu_0 + \pi + \lambda_3\}(r_0 - 1) + \mathcal{P}_2\mathcal{P}_3\mathcal{P}_4\pi\lambda_3}{\mathcal{P}_2\{\alpha\mathcal{P}_4\mathcal{P}_5 + \mathcal{P}_5\lambda\alpha q\lambda_1 + \mathcal{P}_1\mathcal{P}_5\beta q\lambda_1 - \beta q\lambda_1\pi\lambda_3\}}, \quad r^* = \frac{1}{\mu_0}\{\lambda_2 c + (1-q)\lambda_1 a\}, \\
c^* &= \frac{\mathcal{P}_2 q\lambda_1\mu_0\{\mu_0 + \pi + \lambda_3\}(r_0 - 1) + \mathcal{P}_2\mathcal{P}_3\mathcal{P}_4\pi q\lambda_1\lambda_3}{\mathcal{P}_2\{\alpha\mathcal{P}_4\mathcal{P}_5 + \mathcal{P}_5 + \mathcal{P}_5\lambda\alpha q\lambda_1 + \mathcal{P}_1\mathcal{P}_5\beta q\lambda_1 - \beta q\lambda_1\pi\lambda_3\}}, \quad v^* = \frac{1}{\mathcal{P}_5}\{g(1-\eta) + \lambda_3 s\}.
\end{aligned} \tag{18}$$

Now we describe the asymptotic stabilities of the model that is under consideration in the upcoming sections.

2.5. Dynamical properties of the model

We discuss the local analysis of the model to investigate the local asymptotic stability of the proposed problem at $\mathcal{F}_0$ and $\mathcal{F}_1$. To do this, we follow linearization and Routh-Hurwitz criteria. Thus, we state the following results.

Theorem 1. *The proposed model at $\mathcal{F}_0$ is locally asymptotic stable whenever $r_0 < 1$ and $g\eta\varphi > \mu_0 + \mu_1 + \lambda_2$.*

Proof. The characteristic equation of the matrix J at $\mathcal{F}_0$ takes the following form:

$$(\lambda + x_{44})(\lambda^4 + x_1\lambda^3 + x_2\lambda^2 + x_3\lambda + x_4) = 0, \tag{19}$$

where

$$\begin{aligned}
x_1 &= x_{11} + x_{22} + x_{33} + x_{44} + x_{55}, \\
x_2 &= x_{11}x_{22} + x_{11}x_{33} + x_{11}x_{55} + x_{22}x_{55} + x_{33}x_{55} + x_{22}x_{33}(1 - r_1), \\
x_3 &= \mu_0(\mu_0 + \pi + \lambda_3)(x_{22} + x_{33}) + x_{22}x_{33}(x_{11} + x_{55})(1 - r_1), \\
x_4 &= \mu_0(\mu_0 + \pi + \lambda_3)x_{22}x_{33}(1 - r_1).
\end{aligned}$$

Clearly, one eigenvalue λ_1 has negative real part, if $g\eta\varphi > \mu_0+\mu_1+\lambda_2$. For the remaining, if $r_0 < 1$, we have $0 < r_j < 1$, $j = 1, 2$. So $x_i > 0$, for $i = 1, 2, 3, 4$, and $x_1x_2x_3 > x_3^2 + x_1^2x_4$ holds, which implies that the Routh-Hurwitz criterion for stability of the model holds. Hence, the proposed model is locally asymptotically stable at the $\mathcal{F}_0$, if $r_0 < 1$.

Following the same procedure, we can discuss the local dynamics of the model at the endemic state by the subsequent theorem.

Theorem 2. *For $r_0 > 1$, the model is stable locally asymptotically if the following conditions hold:*

1. $\beta\alpha s^* < (1+\beta c^*)(\mu_0+\theta)(\mu_0+\lambda_1)$.
2. $\beta\alpha s^* < (\mu_0+\theta)\{\alpha a^* + \lambda\alpha c^* + (1+\beta c^*)(\mu_0+\lambda_3)\}$.

Proof. The characteristic equation of the matrix J at endemic equilibrium $\mathcal{F}_1$ looks like

$$\lambda^5 + d_1\lambda^4 + d_2\lambda^3 + d_3\lambda^2 + d_4\lambda + d_5 = 0, \tag{20}$$

where

$$\begin{aligned}
d_1 =& x_{11} + x_{22} + x_{33} + x_{44} + x_{55},\\
d_2 =& \{\mu_0+\pi\}x_{21} + \mu_0\{\mu_0+\lambda_3+\pi\} + x_{11}x_{22} + x_{11}x_{33} + x_{11}x_{44} + x_{22}x_{33} + x_{22}x_{44}\\
&+ x_{22}x_{55} + x_{33}x_{44} + x_{33}x_{55} + x_{44}x_{55} - \theta x_{22},\\
d_3 =& \theta q\lambda_1 x_{24} + x_{11}\{x_{22}x_{33} - \theta x_{23}\} + x_{44}\{x_{11}x_{22} - \theta x_{23}\} + x_{11}x_{33}x_{44} + \theta x_{21}x_{13}\\
&+ \{x_{22} + x_{33} + x_{44}\}\{(\mu_0+\pi) + \mu_0(\mu_0+\pi+\lambda_3)\} + x_{55}\{x_{22}x_{33} - \theta x_{23}\}\\
&+ x_{22}x_{44}x_{55} + x_{33}x_{44}x_{55} + x_{22}x_{33}x_{44} + x_{21},\\
d_4 =& \theta x_{21}x_{31}x_{55} + \{(\mu_0+\pi)x_{21} + \mu_0(\mu_0+\pi+\lambda_3)\}\{x_{22}x_{33} + x_{22}x_{44} + x_{33}x_{44}\}\\
&+ \theta q\lambda_1(x_{55} - x_{14}) + x_{44}x_{55}(x_{22}x_{33} - \theta x_{23}) + x_{11}x_{44}\{x_{22}x_{33} - \theta x_{23}\} + \theta x_{21}x_{13}x_{44}\\
&+ \theta\pi\lambda_3 x_{23} + \theta q\lambda_1 x_{11}x_{24} - \theta x_{11}x_{23}x_{55},\\
d_5 =& \{(\mu_0+\pi)x_{21} + \mu_0(\mu_0+\pi+\lambda_3)\}x_{22}x_{33}x_{44} + \theta\lambda_3\pi x_{23}x_{44}\theta\lambda_3\pi q\lambda_1 x_{24}\\
&+ \theta q\lambda_1 x_{55}\{x_{11}x_{24} - x_{14}\} + \theta x_{13}x_{24}x_{44}x_{55} - \theta x_{11}x_{23}x_{44}x_{55}.
\end{aligned}$$

All $d_i > 0$, for $i = 1,2,3,4,5$ and

$$\begin{aligned}
\mathcal{H}_0 : \big\{ & r_0 > 1,\ d_1d_2d_3 > d_3^2 + d_1^2d_4,\\
& (d_1d_4 - d_5)\left(d_1d_2d_3 - d_3^2 - d_1^2d_4\right) > d_5\left(d_1d_2 - d_3^2\right)^2 + x_1x_5^2\big\},
\end{aligned}$$

holds implies that $\mathcal{H}_0$ is satisfied if conditions 1 and 2 hold. Thus, it ensures that the Routh-Hurwitz stability criteria are satisfied, and we conclude that the endemic state $\mathcal{F}_1$ is locally asymptotically stable.

Upon establishing the analytical results, we now proceed to numerically simulate the model in order to validate our theoretical findings, as detailed in the following section.

3. Numerical simulation

In this section, we carry out numerical experiments to validate the analytical results and demonstrate the robustness of the proposed hybrid approach. We begin by discretizing the model using the nonstandard finite difference (NSFD) scheme, followed by a summary of the architecture of the proposed feed-forward neural network (FFNN).

3.1. Non-standard finite difference scheme and the architecture of the neural network

In this section, we present the model discretization with the aid of NSFD and provide the architecture of the neural network that will be used for the learning process. It is obvious that the proposed model has six state variables i.e. $s(t)$, $l(t)$, $a(t)$, $c(t)$, $r(t)$, and $v(t)$, and g, η, π, α, β, λ, λ_1, λ_2, λ_3, μ_0, θ, q and μ_1 are the parameters. To approximate the model, we use a non-standard finite difference scheme given by

$$y_{n+1} = y_n + \Delta t.h(y_n), \tag{21}$$

for every $y \in \{s, l, a, c, r, v\}$, and $h(y_n)$ represents the right side of proposed model. Let Δt is the discrete time step represent the approximation at $t = n\Delta t$, then

$$s_n \approx s(n\Delta t), \quad l_n \approx l(n\Delta t), \quad a_n \approx a(n\Delta t), \quad c_n \approx c(n\Delta t), \quad r_n \approx r(n\Delta t), \quad v_n \approx v(n\Delta t).$$

Using NSFD discretization, the proposed model takes the following form

$$\begin{aligned}
s_{n+1} &= s_n + \Delta t \left\{ g\eta(1 - \varphi c_n + \pi v_n) - \frac{\alpha s_n a_n}{1 + \beta c_n} - \frac{\lambda \alpha s_n c_n}{1 + \beta c_n} - (\mu_0 + \lambda_3) s_n \right\}, \\
l_{n+1} &= l_n + \Delta t \left\{ \frac{\alpha s_n a_n}{1 + \beta c_n} + \frac{\lambda \alpha s_n c_n}{1 + \beta c_n} - (\mu_0 + \theta) l_n \right\}, \\
a_{n+1} &= a_n + \Delta t \left\{ \theta l_n - (\mu_0 + \lambda_1) a_n \right\}, \\
c_{n+1} &= c_n + \Delta t \left\{ g\eta\varphi c_n + q\lambda_1 a_n - (\mu_0 + \mu_1 + \lambda_2) c_n \right\}, \\
r_{n+1} &= r_n + \Delta t \left\{ \lambda_2 c_n + (1 - q)\lambda_1 a_n - \mu_0 r_n \right\}, \\
v_{n+1} &= v_n + \Delta t \left\{ g(1 - \eta) + \lambda_3 s_n - (\mu_0 + \pi) v_n \right\}.
\end{aligned} \tag{22}$$

Using the hypothetical values of the model parameters as: $g = 0.7$, $\eta = 0.85$, $\varphi = 0.05$, $\pi = 0.08$, $\alpha = 0.4$, $\beta = 0.15$, $\lambda = 0.35$, $\lambda_1 = 0.12$, $\lambda_2 = 0.06$, $\lambda_3 = 0.03$, $\mu_0 = 0.02$, $\theta = 0.15$, $q = 0.75$, $\mu_1 = 0.025$. To approximate the proposed system numerically, we then use a standard feed-forward neural network (FFNN) with one hidden layer consisting of input layer $t \in R$, number of neurons $n_h = 10$, and activation function (ReLU) $\sigma(.)$. Let $W^{(1)} \in R^{n_h \times 1}$ represent the weights from input to the hidden layer and $b^{(1)} \in R^{n_h}$ is the biases in the hidden layer, then the hidden layer out is given by

$$h = \sigma\left(W^1 t + b^{(1)}\right) \in \mathcal{R}^{n_h}. \tag{23}$$

Likewise, the output layer is a six-dimensional vector (s, l, a, c, r, v). Let $W^{(2)} \in R^{6 \times n_h}$ represent the weights from hidden to output layer, and $b^2 \in R^6$ represent the biases in output layer. Then the predicted output becomes

$$\hat{y}(t) = W^{(2)} h + b^{(2)} \in \mathcal{R}^6. \tag{24}$$

Combining all, we get the following expression

$$\hat{y}(t) = W^{(2)} h \sigma\left(W^{(1)t} + b^{(1)}\right) + b^{(2)}, \tag{25}$$

where $\hat{y}(t) = \left[\hat{s}(t), \hat{l}(t), \hat{a}(t), \hat{c}(t), \hat{r}(t), \hat{v}(t)\right]^t$ and $\sigma(.)$ is the activation function. Further, to minimize the Mean Squared Error (MSE), we train the network to minimize the error between the true and predicted values over the training set $\{(t_i, y_i)\}_{i=1}^{N}$, which is given by

$$MSE = \frac{1}{6N} \sum_{i=1}^{N} \|y_i - \hat{y}(t_i)\|^2, \tag{26}$$

where $y_i = [s(t_i), l(t_i), a(t_i), c(t_i), r(t_i), v(t_i)]^t$ and $\hat{y}(t_i)$ is the network output.

3.2. Numerical experiment

To perform the numerical experiment, we use the discretized system (22) to generate the data for the learning process, and then use a feed-forward neural network (FFNN) to forecast the dynamics of the proposed model in the long run. For each state (s, l, a, c, r, v) of the model, we present the dynamics as reported in Figures 2 to 7. Each figure represents the dynamics of the compartmental population of the proposed model with absolute error. The blue line demonstrates the true values of the model states over time using NSFD, and the red dashed line shows the predicted values of the model states over time using FFNN. Clearly, the results show how the true and approximated values are closer because the blue line follows the red-dashed line, which guarantees a better prediction. We also provided the associated absolute error graphs as shown by a magenta line for each state of the model, which shows the magnitude of error, describing how far off the prediction is (see Figures 2 to 7).

To quantify the overall error prediction for each model state variable (s, l, a, c, r, and v), a Mean Square Error (MSE) bar graph is presented as shown by Figure 8. This provides the overall performance of the proposed FFNN on each state variable. On the x-axis, the indices of the variables s, l, a, c, r, and v are taken, while on the y-axis, the Mean Square Error (MSE) values are plotted, which clearly shows that the low MSE guarantees better FFNN performance. In addition, the validation checks, damping factor (μ), and Gradient interpretation are provided as shown in Figure 9. More precisely, this demonstrates the performance of the validation set against epochs. Every time the check occurs, if the performance fails to improve for a specific number of epochs, however, the training stops, if the performance on these validations set does not improve over these checks. Also, to show the training efficiency, the damping factor μ is visualized as shown in Figure 9. Similarly, to show the performance of the gradient with respect to the biases and weights, that is, how steep the slope is at the current point in the error surface, we interpret the gradient. In the end, the regression plots are provided for the FFNN training to present the correlation between the actual and predicted values for the data set and R-value as illustrated in Figure 9, which shows the performance of the trained FFNN. In every subplot of Figure 10, representing perfect agreement. The regression lines fitted to the data lie almost exactly on the identity line, with negligible intercepts, suggesting minimal prediction bias. Moreover, the close alignment verifies that the network has learned well the underlying mapping with high precision. The results highlight the accuracy and robustness of the

hybrid approach of NSFD–FFNN, demonstrating its effectiveness in capturing the complex nonlinear dynamics of the modeled system.

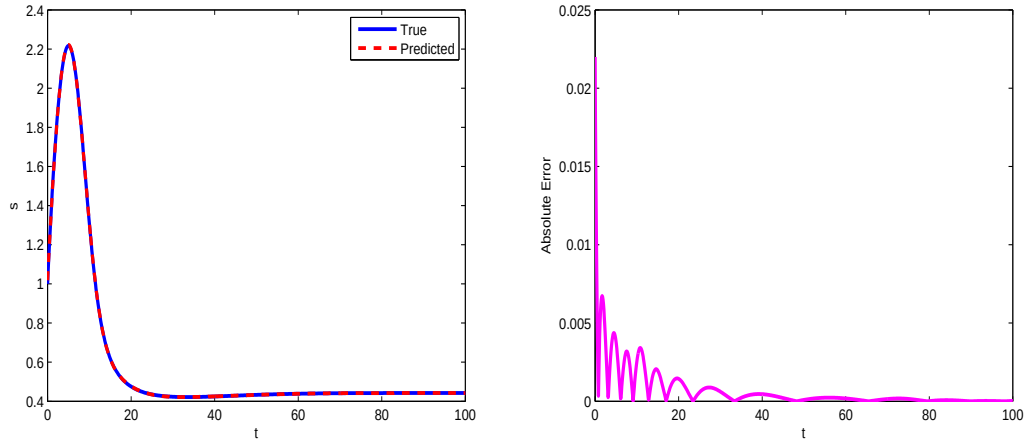

Figure 2: The graphs represents the temporal dynamics of the state s and its associated absolute error.

Overall, we observe that the feed-forward neural network (FFNN) learned from the data simulated by NSFD exhibits an excellent learning and generalization capacity. The validation checks describe minimal overfitting, and the trajectory of the damping factor (μ) shows adaptive learning and stable behavior, as well as effective convergence, as seen by the gradient descent pattern. The regression analysis shows that the clustering of points around the diagonal line indicates that the proposed network has efficiently captured the nonlinear dynamics of the proposed epidemiological model simulated by NSFD, which confirms the robustness of the underlying hybrid NSFD–FFNN framework.

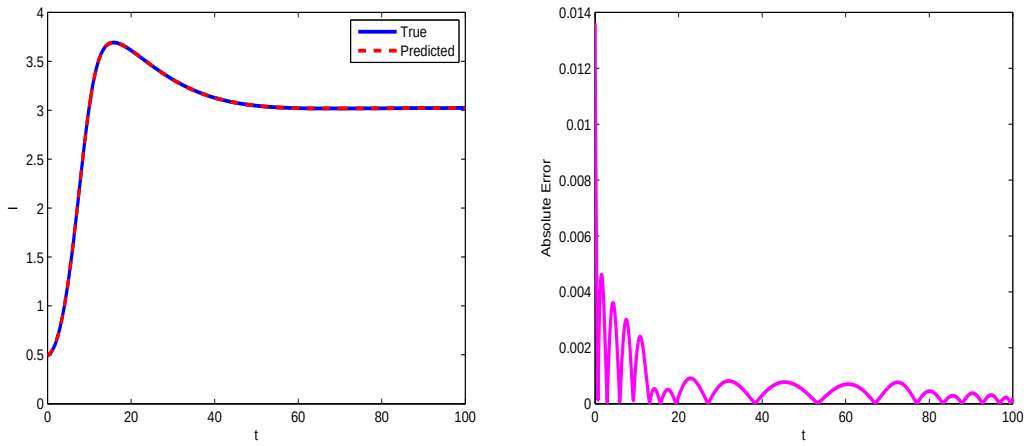

Figure 3: The time dynamics of the state I with its absolute error.

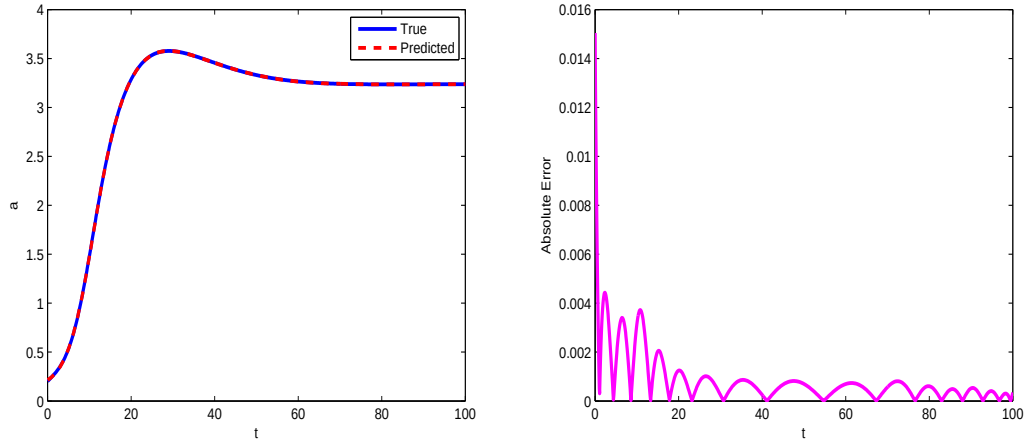

Figure 4: This demonstrate the dynamics of state a and its absolute error.

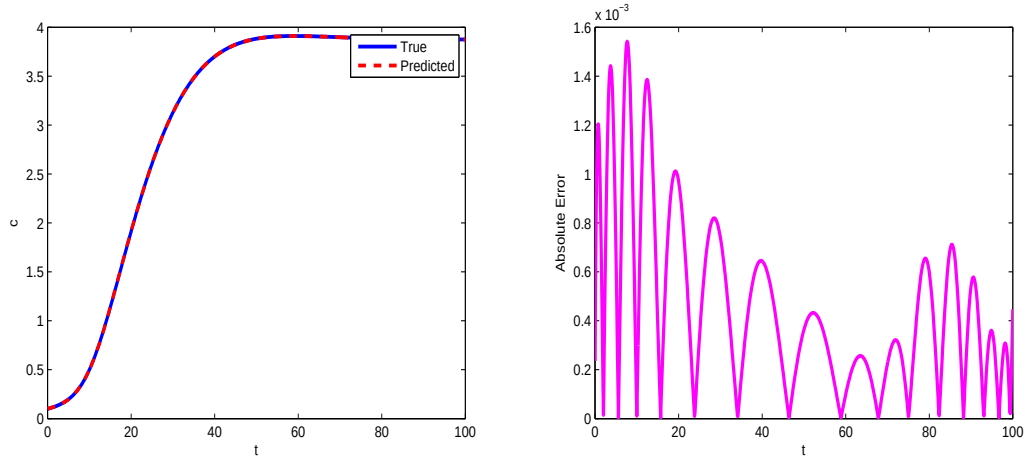

Figure 5: The graphs visualizes the dynamics of the model state c with its associated absolute error.

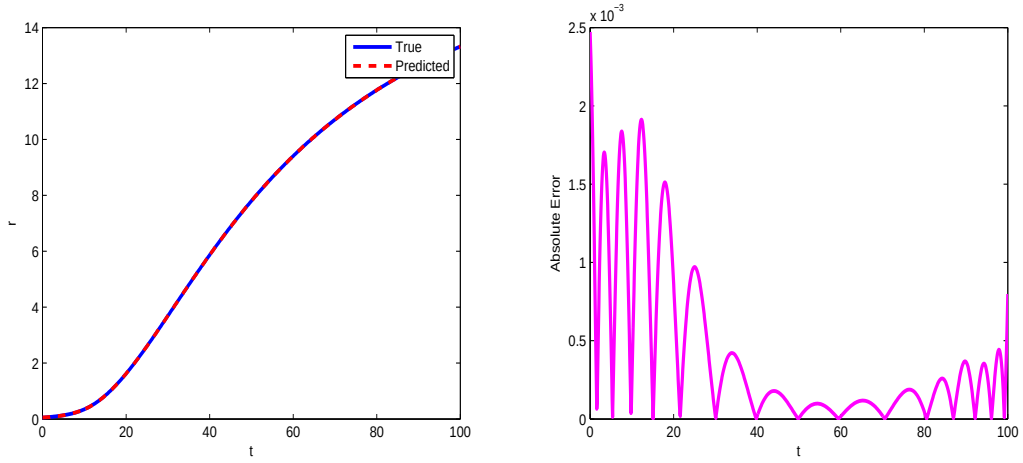

Figure 6: Dynamics of the model state r with absolute error.

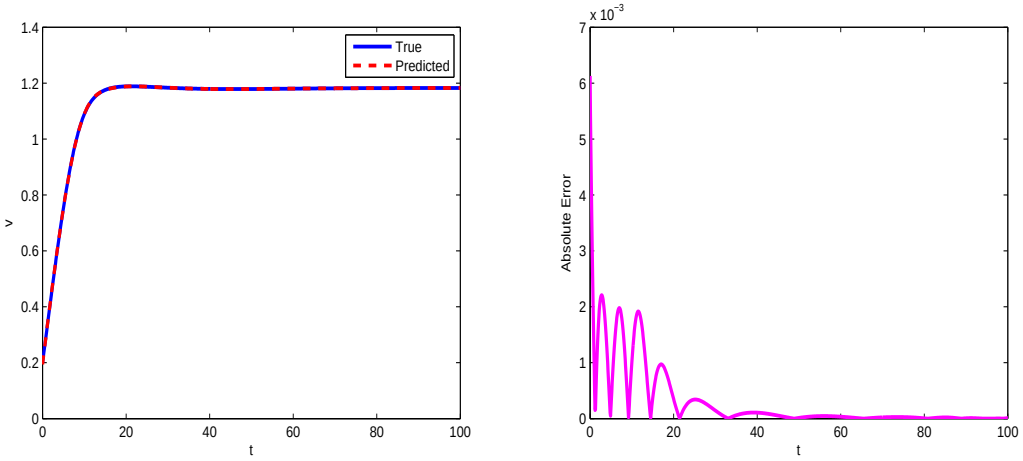

Figure 7: The dynamics of the model state v with its associated absolute error.

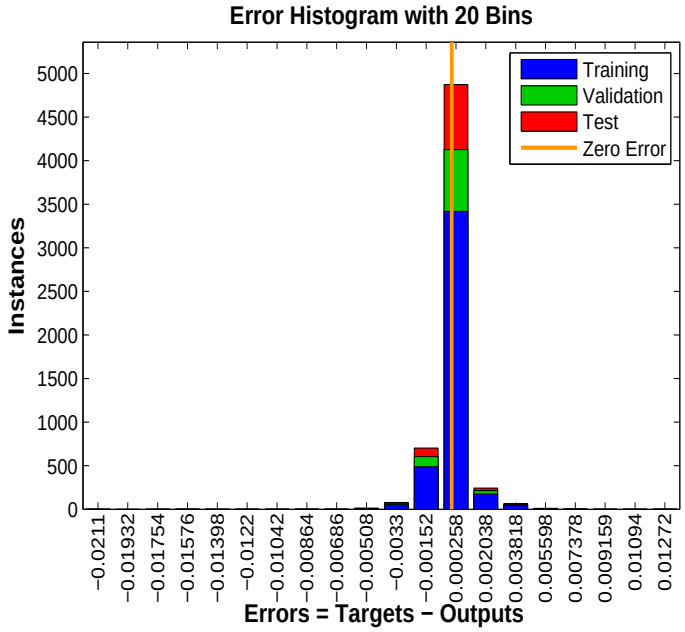

Figure 8: The graphs show time dynamics of the compartmental population of the model that is under consideration at the disease free equilibrium state.

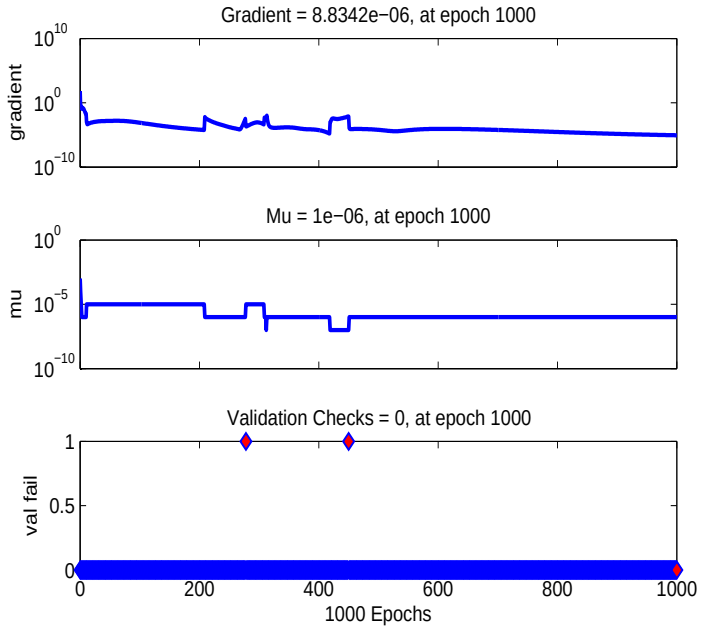

Figure 9: The graphs show time dynamics of the compartmental population of the model that is under consideration at the disease free equilibrium state.

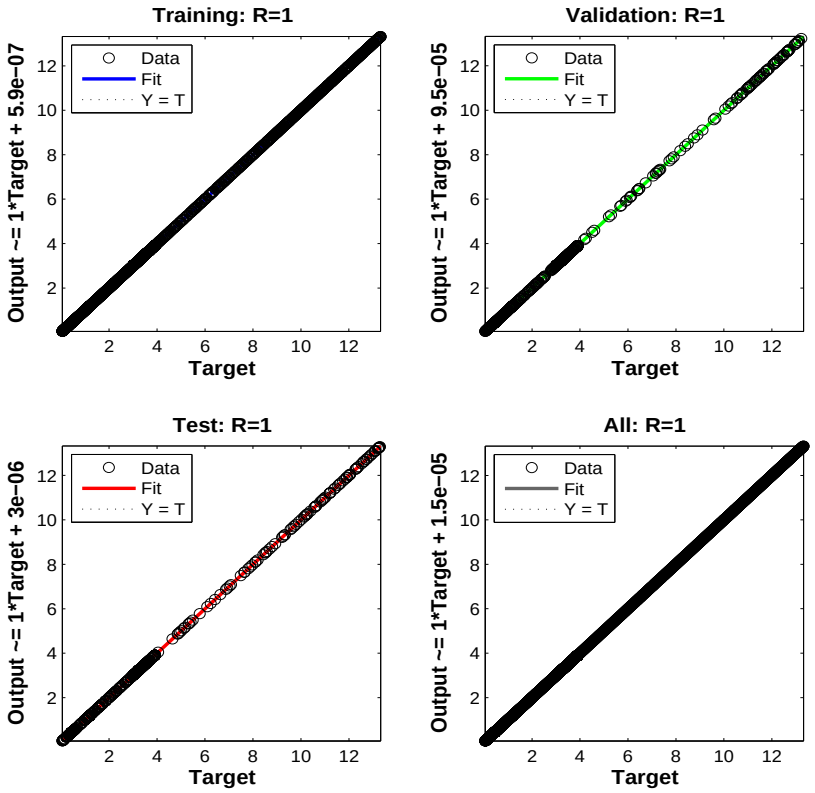

Figure 10: The graphs show time dynamics of the compartmental population of the model that is under consideration at the disease free equilibrium state.

4. Conclusion

In this paper, we investigated the transmission dynamics of hepatitis B virus (HBV) using the integration of an epidemic model FFNN. The model has been carefully constructed to reflect the key biological features of HBV, including its various infection stages (latent, acute, and chronic), as well as a saturated incidence rate to capture the behavioral and healthcare constraints associated with HBV transmission. We established the well-posedness of the model to ensure biological and mathematical feasibility of the problem. We also derived the basic reproduction number, and studied a comprehensive stability analysis to assess the conditions under which the disease-free and endemic states are stable. To validate the analytical findings and explore the model's behavior, we employed a novel hybrid numerical framework combining the nonstandard finite difference (NSFD) scheme with a feed-forward neural network (FFNN). The numerical results demonstrated a high degree of accuracy, evidenced by low mean squared error and a strong agreement between the true trajectories produced by NSFD and predicted trajectories provided by

FFNN. This confirms the robustness and reliability of both the proposed model and the computational approach. The study not only provides valuable insights into the complex dynamics of HBV transmission but also provides evidence of the effectiveness of a hybrid approach capturing the progression of infectious diseases. Moreover, the proposed approach is computationally stable, sound, and adaptable, which offers a promising tool for other epidemiological models.

In future, we will extend the model to incorporate the stochastic perturbation to capturing disease uncertainty in heterogeneous environments, and the integrate it with machine learning with the help of feed-forward neural network. The FFNNs will be used to learn the underlying nonlinear dynamics governed by the associated stochastic differential equations (SDEs) and predict for the long run.

Acknowledgements

This work was supported by the National Research Foundation of Korea (NRF) Grant funded by the Korean Government (MSIT) (No. RS-2024-00342113 and 2022R1A5A1033624).

References

[1] Scott D Holmberg, Anil Suryaprasad, and John W Ward. Updated cdc recommendations for the management of hepatitis b virus infected health care providers and students. 2012.

[2] Sonia Altizer, Andrew Dobson, Parviez Hosseini, Peter Hudson, Mercedes Pascual, and Pejman Rohani. Seasonality and the dynamics of infectious diseases. *Ecology letters*, 9(4):467–484, 2006.

[3] Brian J McMahon. Epidemiology and natural history of hepatitis b. In *Seminars in liver disease*, volume 25, pages 3–8. Published in 2005 by Thieme Medical Publishers, Inc., 333 Seventh Avenue . . . , 2005.

[4] Yukihiko Nakata and Toshikazu Kuniya. Global dynamics of a class of seirs epidemic models in a periodic environment. *Journal of Mathematical Analysis and Applications*, 363(1):230–237, 2010.

[5] Marc Ringehan, Jane A McKeating, and Ulrike Protzer. Viral hepatitis and liver cancer. *Philosophical Transactions of the Royal Society B: Biological Sciences*, 372(1732):20160274, 2017.

[6] Abubakar Mwasa and Jean M Tchuenche. Mathematical analysis of a cholera model with public health interventions. *Biosystems*, 105(3):190–200, 2011.

[7] Tailei Zhang, Kai Wang, and Xueliang Zhang. Modeling and analyzing the transmission dynamics of hbv epidemic in xinjiang, china. *PloS one*, 10(9):e0138765, 2015.

[8] Kamil Shah, Jamal Shah, Ebenezer Bonyah, Tmader Alballa, Hamiden Abd El-Wahed Khalifa, Usman Khan, and Hameed Khan. Optimal control of covid-19 through strategic mathematical modeling: Incorporating harmonic mean incident rate and vaccination. *AIP Advances*, 14(9), 2024.

[9] Muhammad Farhan, Fahad Aljuaydi, Zahir Shah, Ebraheem Alzahrani, Ebenezer Bonyah, and Saeed Islam. A fractional modeling approach to a new hepatitis b model in light of asymptomatic carriers, vaccination and treatment. *Scientific African*, 24:e02127, 2024.

[10] Lan Zou, Weinian Zhang, and Shigui Ruan. Modeling the transmission dynamics and control of hepatitis b virus in china. *Journal of theoretical biology*, 262(2):330–338, 2010.

[11] Junjie Zhu, Misbah Ullah, Saif Ullah, Muhammad Bilal Riaz, Abdul Baseer Saqib, Atif M Alamri, and Salman A AlQahtani. A novel numerical solution of nonlinear stochastic model for the propagation of malicious codes in wireless sensor networks using a high order spectral collocation technique. *Scientific Reports*, 15(1):228, 2025.

[12] Anwarud Din and Yongjin Li. Optimizing hiv/aids dynamics: stochastic control strategies with education and treatment. *The European Physical Journal Plus*, 139(9):812, 2024.

[13] Wan Yang, Alicia Karspeck, and Jeffrey Shaman. Comparison of filtering methods for the modeling and retrospective forecasting of influenza epidemics. *PLoS computational biology*, 10(4):e1003583, 2014.

[14] Suthep Suantai, Zulqurnain Sabir, Muhammad Asif Zahoor Raja, and Watcharaporn Cholamjiak. A stochastic bayesian neural network for the mosquito dispersal mathematical system. *Fractal and Fractional*, 6(10):604, 2022.

[15] Atifa Asghar, Mohsan Hassan, Zulqurnain Sabir, Shahid Ahmad Bhat, and Sharifah E Alhazmi. A design of computational stochastic framework for the mathematical severe acute respiratory syndrome coronavirus model. *Biomedical Signal Processing and Control*, 100:107049, 2025.

[16] Muhammad Farhan, Saif Ullah, Waseem, Muath Suliman, Abdul Baseer Saqib, and Mohammed Qeshta. Deep learning-driven insights into the transmission dynamics of hepatitis b virus with treatment. *Scientific Reports*, 15(1):23741, 2025.

[17] Zulqurnain Sabir, Thongchai Botmart, Muhammad Asif Zahoor Raja, R Sadat, Mohamed R Ali, Abdulaziz A Alsulami, Abdullah Alghamdi, et al. Artificial neural network scheme to solve the nonlinear influenza disease model. *Biomedical Signal Processing and Control*, 75:103594, 2022.

[18] Kanit Mukdasai, Zulqurnain Sabir, Muhammad Asif Zahoor Raja, Peerapongpat Singkibud, R Sadat, and Mohamed R Ali. A computational supervised neural network procedure for the fractional siq mathematical model. *The European Physical Journal Special Topics*, 232(5):535–546, 2023.

[19] Muhammad Farhan, Zhi Ling, Saif Ullah, Almetwally M Mostafa, Salman A AlQahtani, et al. A novel intelligent framework for assessing within-host transmission dynamics of chikungunya virus using an unsupervised stochastic neural network approach. *Computational Biology and Chemistry*, 117:108380, 2025.

[20] Jamiu Adeyemi Ademosu, Samson Olaniyi, Sulaimon Femi Abimbade, Furaha Michael Chuma, Richard Chinedu Ogbonna, Ramoshweu Solomon Lebelo, and Kazeem Oare Okosun. Modelling population dynamics of substance abuse in the presence of addicted immigrant with real data of rehabilitation cases. *Journal of Applied*

Mathematics, 2025(1):2241780, 2025.

[21] Pauline Van den Driessche and James Watmough. Reproduction numbers and subthreshold endemic equilibria for compartmental models of disease transmission. *Mathematical biosciences*, 180(1-2):29–48, 2002.